PAPER

Temperature invariant lifetime based luminescent manometer on Mn^{4+} ions†

M. Pieprz,[a] M. Runowski, [iD][bc] P. Woźny, [iD][b] J. Xue[d] and L. Marciniak [iD] *[a]

Luminescent manometry enables remote pressure readout with unprecedented spatial and pressure resolution. The need to image pressure in a temperature-invariant manner imposes the search for new solutions that offer such capabilities. In this study, we present an approach that enables remote pressure sensing using the luminescence kinetics of Mn^{4+} ions in SrGdAlO$_4$. The uniqueness of this solution is related to the pressure induced prolongation of the lifetime of the ^{2}E level of Mn^{4+} ions resulting from a change in the covalency of the Mn^{4+}–O^{2-} bond. Taking the advantage of this effect, the luminescence decay time was increased from 1.44 ms to 2.14 ms when the pressure was changed from ambient to 7.6 GPa. This allowed the development of a luminescent manometer with a maximum relative sensitivity of 7.85%/GPa at 3 GPa and sensitivities above $S_R > 5\%$/GPa in the pressure range of 1–7.6 GPa. Moreover, in the temperature range of 260–365 K, the lifetime value was independent of temperature changes, enabling a temperature invariant manometric factor of 134.

Introduction

Apart from the lighting market, luminescent materials are increasingly finding new applications, among which the sensing market has recently been one of the most developed owing to their ability to readout and even image physical and chemical quantities of objects under study, which can be done remotely by analyzing the spectroscopic parameters associated with the emitted light.[1–6] In addition to the most popular luminescence thermometry, the possibility of remote pressure monitoring has also been intensively explored recently.[7–11] Among the luminescent manometers described so far, the most common way to readout the pressure values in a given system is through spectral band shift analysis.[11–26] This strategy applies both to luminophores with a narrow emission band headed by ruby and also to broadband luminophores. In this case, the pressure reading involves either an analysis of the position of the emission band centroid or a ratiometric reading of the ratio of luminescence intensities occurring in the two spectral bands.[9,11,19–22] However, in the case of applications of luminescent manometers in environments where the medium is characterized by a dispersive dependence of the extinction coefficient, a reading based on analysis of the spectral response, including ratiometric approach and the band shift of the luminophore can lead to reduced reliability owing to the interactions of the emitted light with the medium in the form of absorption and/or scattering.[23,24] Hence, in such applications, luminescent manometers using pressure-induced changes in luminescence kinetics are advantageous. Importantly and often overlooked, a luminescent pressure gauge should be characterized by insensitivity to temperature changes so that the pressure reading offered is unambiguous, even under extreme conditions of pressure and temperature. Although this type of manometer is rarely described in the literature, the vast majority of them are based on the luminescence of Ln^{3+} ions, where the dominant processes affecting the shortening of a lifetime are multiphonon and cross-relaxations,[25] and their probabilities are significant for most Ln^{3+} ions at room temperature. This makes an unambiguous pressure reading difficult. On the other hand, due to the shielding of the 4f subshell by external orbitals, an increase in pressure does not significantly change the probability of radiative processes, hence little change in luminescence kinetics under increasing pressure is observed. Therefore, herein, we propose a new approach, in which we take the advantage of the fact that the spectroscopic properties of transition metal ions significantly depend on the strength of the crystal field, and therefore, on the applied pressure to lifetime-based manometers. Mn^{4+} ions, which are known for their red emission associated with the ^{2}E → ^{4}A$_2$ electron transition, were used as model ions in this case.[26–28]

[a] *Institute of Low Temperature and Structure Research, Polish Academy of Sciences, Okólna 2, Wrocław 50-422, Poland. E-mail: l.marciniak@intibs.pl*

[b] *Adam Mickiewicz University, Faculty of Chemistry, Uniwersytetu Poznańskiego 8, Poznań 61-614, Poland*

[c] *Departamento de Física, Instituto de Materiales y Nanotecnología, IUdEA & MALTA Consolider Team, Universidad de La Laguna, Apdo. Correos 456, San Cristóbal de La Laguna E-38200, Santa Cruz de Tenerife, Spain*

[d] *Department of Physics, Pukyong National University, Busan 608-737, Republic of Korea*

† Electronic supplementary information (ESI) available. See DOI: https://doi.org/10.1039/d3tc00911d

This journal is © The Royal Society of Chemistry 2023

J. Mater. Chem. C, 2023, **11**, 11353–11360 | **11353**

For Mn^{4+} ions, the rate of depopulation of the excited ^2E level depends on the relative energy distance between the ^2E level and the intersection point with the $^4T_2$ state. The energy of the $^4T_2$ state increases with increasing crystal field strength, hence it is expected that as the applied pressure increases the probability of the non-radiative processes will decrease, leading to the prolongation of the luminescence lifetime. In addition, a change in the applied pressure will affect the covalency of the $Mn^{4+}-O^{2-}$ bond by changing the probability of non-radiative processes. The energy of the $^4T_2$ level of Mn^{4+} ions significantly depends on the strength of the crystal field acting on it and thus depends on the applied pressure.

Experimental

$SrGdAlO_4$ powders doped with different concentrations of Mn^{4+} ions were synthesized by a modified Pechini method.[29] The materials used for synthesis: strontium nitrate ($Sr(NO_3)_2$ 99.9965% purity from AlfaAesar), aluminum nitrate hydrate ($Al(NO_3)_3 \cdot 9H_2O$ 99.999% purity from AlfaAesar), gadolinium oxide (Gd_2O_3 99.995% purity from Stanford Materials Corporation), manganese(II) chloride tetrahydrate ($MnCl_2 \cdot 4H_2O$ 99% purity from Sigma Aldrich), nitric acid (HNO_3 65%; pure p.a.; from POCH), citric acid ($\geq$99.5%, Sigma–Aldrich) and polyethylene glycol PEG 200 ($H(OCH_2CH_2)_nOH$, $n = 200$, Alfa Aesar) were used without further purification. First, a stoichiometric amount of gadolinium oxide was dissolved in nitric acid to obtain gadolinium nitrate. Then, a three-fold recrystallization was carried out to evaporate the excess nitric acid. Appropriate amounts of strontium nitrate, aluminum nitrate, and manganese chloride were added to the gadolinium precursor and dissolved in 50 ml of distilled water. Next, citric acid was added in an amount six times the number of moles of the metal ions used in the synthesis. Once a clear solution was obtained, PEG was added in a 1:1 ratio to the citric acid, and stirring continued for 2 h at room temperature. After this, the mixture was transferred to a porcelain crucible and dried at 360 K for 7 days. The obtained resin was then quenched at 873 K for 3 h, followed by grating in a mortar under hexane. This was placed in a crucible and annealed at 1323 K for 5 h in air.

The obtained materials were then examined by X-ray powder diffraction (XRD) using a PANalytical X'Pert Pro diffractometer in Bragg–Brentano geometry equipped with an Anton Paar TCU1000 N temperature control unit using Ni-filtered Cu Kα radiation ($V = 40$ kV, $I = 30$ mA). Measurements were made in the range of 10–90°, and the acquisition time was approximately 30 min. Transmission electron microscopy (TEM) images were taken using a Philips CM-20 SuperTwin TEM microscope. The samples were dispersed in methanol, and a droplet of such suspension was put on a microscope copper grid. Next, the samples were dried and purified in a plasma cleaner. Studies were performed in a conventional TEM procedure with 160 kV parallel beam electron energy. The sizes were determined manually using ImageJ software by measuring the longest linear size (Feret diameter) of each particle.

Excitation and emission spectra were measured on a FLS1000 spectrometer from Edinburgh Instruments supplied with a 450 W xenon lamp as an excitation source, and a R928P side window photomultiplier tube from Hamamatsu as a detector. The temperature dependent emission spectra and luminescence decay profile were measured using the same system with a 445 nm laser diode from CNI Lasers used as the excitation source and a THMS 600 heating–cooling stage from Linkam to control the temperature with a precision of 0.1 K. Luminescence spectra and luminescence decay profile as a function of pressure were measured using the same excitation source. Pressure was applied to the sample owing to a gas membrane that transmitted it to the Diacell μScopeDAC-RT(G) diamond anvil cell (DAC) with 0.4 mm diamond culets. The gas used in the system is compressed nitrogen, which was supplied to the membrane using a Druck PACE 5000 which allowed for a relatively controlled change in pressure. Since the emission band of the Cr^{3+} ions of $Al_2O_3:Cr^{3+}$ spectrally overlaps with the emission band of the analyzed $SrGdAlO_4:Mn^{4+}$, the spectral shift of the $SrB_4O_7:Sm^{2+}$ $^5D_0 \rightarrow {}^7F_0$ emission line was used as a pressure indicator in the DAC.[30] The sample was placed in a $\approx$140 μm size hole drilled in a 250 μm thick stainless steel gasket. The methanol–ethanol solution (4:1 ratio) was used as a pressure transmission medium. The Raman spectra were measured in the pressure range from $\approx$0 to 9 GPa, in a backscattering geometry using a Renishaw InVia confocal micro-Raman system with a power-controlled 100 mW 532 nm laser diode. The laser beam was focused using an Olympus x20 SLMPlan N long working distance objective. The Raman spectra of the sample compressed in a methanol/ethanol/water – 16/3/1 (pressure transmitting medium) were measured in a DAC equipped with ultra-low fluorescence (IIas) diamond anvils.

Results and discussion

The $SrGdAlO_4$ compound crystallizes in a tetragonal structure with the space group $I4/mmm$ ($a = b = 0.3663$ nm, $c = 1.1998$ nm, $\alpha = \beta = \gamma = 90°$).[31–37] In this host material, Sr^{2+} and Gd^{3+} are nine-fold coordinated, whereas Al^{3+} ions are surrounded by six oxygen atoms forming $(AlO_6)^{9-}$ octahedrons (Fig. 1a). Mn^{4+} ions, due to the ionic radius ($r_{Mn^{4+}} = 0.530$ Å) and preferred coordination number (CN = 6), effectively substitute the Al^{3+} site ($r_{Al^{3+}} = 0.535$ Å CN = 6) of the C_{4v} point symmetry in the $SrGdAlO_4$ structure. Hence, no significant changes in the XRD patterns are observed for different concentrations of Mn^{4+} ions (Fig. 1b). All the diffraction reflexes correlate with the reference pattern for the bulk $SrNdAlO_4$ (JCPDS no. 24-1185) confirming the lack of additional phases in the sample. The Rietveld analysis of the obtained diffractograms reveals that the c parameters slightly decrease with the increase of the Mn^{4+} concentration (Fig. 1c), while the a parameter remains independent of dopant concentration (Fig. 1d). The slight shrinkage of the c parameter results from the ionic difference between Mn^{4+} and the Al^{3+} ions. The morphological studies of the

11354 | *J. Mater. Chem. C*, 2023, **11**, 11353–11360

This journal is © The Royal Society of Chemistry 2023
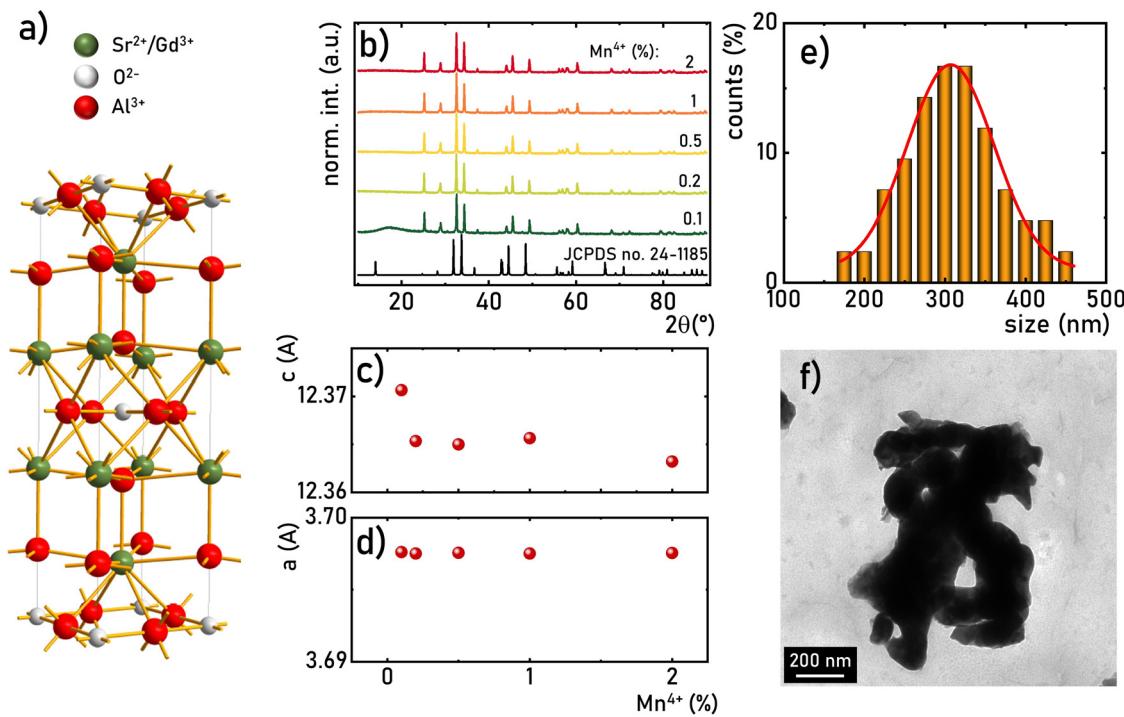
Fig. 1 Visualization of the crystal structure of the $SrGdAlO_4$ material (a); XRD patterns of the $SrGdAlO_4$: Mn^{4+} for different concentrations of dopant ions (b); calculated c (c) and a (d) parameters for the $SrGdAlO_4$: Mn^{4+} material as a function of Mn^{4+} concentration; particle size distribution (d_{avr} = 306 nm, FWHM = 98 nm) (e) and representative TEM image (f) of the $SrGdAlO_4$: 0.2%Mn^{4+}.
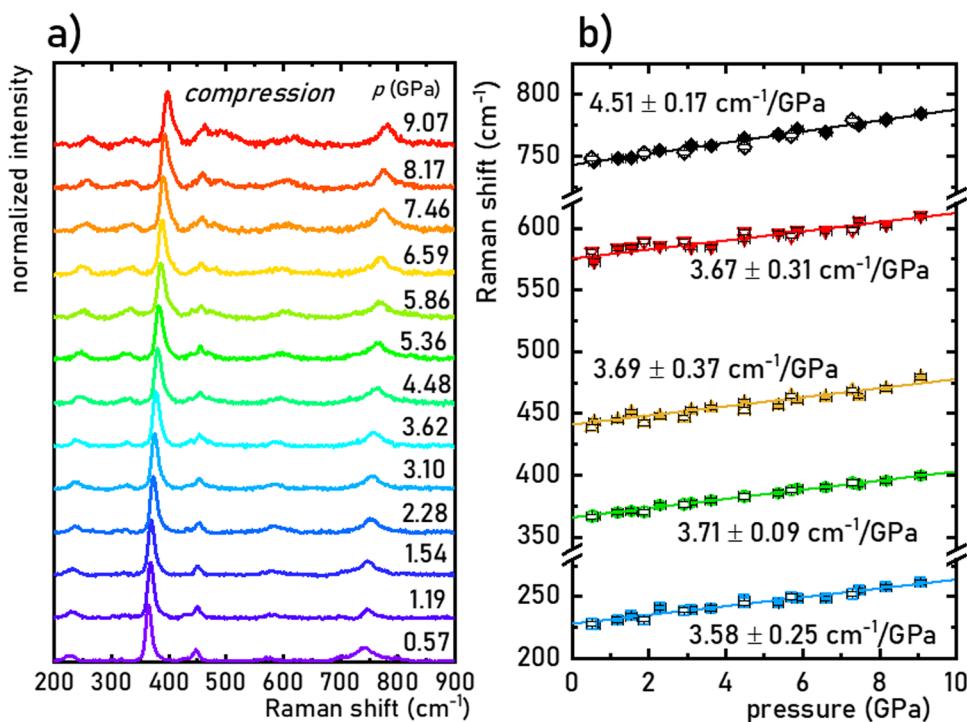
Fig. 2 Normalized Raman spectra for the $SrGdAlO_4$ material measured for different pressure values, during the compression cycle (a); determined energies (peak centroids) of the most intense phonon modes as a function of pressure (b); filled symbols represent compression data and empty ones represent decompression data; the continuous lines are the linear fits applied for determination of the pressure shift rates of the corresponding Raman modes.

This journal is © The Royal Society of Chemistry 2023

J. Mater. Chem. C, 2023, **11**, 11353–11360 | **11355**

SrGdAlO$_4$:Mn^{4+} material performed based on the TEM images, indicate that the obtained powder samples consist of well-crystalized particles of around 300 nm in diameter, (Fig. 1e, see also Fig. S1, ESI†) with a high degree of aggregation (Fig. 1f).

The structural stability of the SrGdAlO$_4$ material was investigated by measuring the Raman spectra for the undoped compound, to avoid luminescence from the activator ions, which often obscure and superimpose with Raman peaks. The measured Raman spectrum for the SrGdAlO$_4$ material at low pressure has five bands initially located around ≈230, 370, 440, 575, and 740 cm^{-1}, as shown in Fig. 2a and b. With increasing pressure (material compression) the energies of the phonon modes increase, and the corresponding Raman bands shift towards higher wavenumbers, as shown in Fig. 2b. The observed effect originates from the bonds shortening, *i.e.*, the decrease of the interatomic distances in the compressed structures. It is worth noting that the determined spectral shifts are monotonous and linear, which assure good structural stability of the investigated materials. The calculated shift rates (cm^{-1}/GPa) for the observed Raman peaks are given in Table S1 in the ESI† data. Note that the observed deterioration of the Raman signal with pressure (lowering signal-to-noise ratio) is associated with increasing strains and crystal defects in the compressed crystal structures, which is typically observed for Raman measurements. Importantly, on releasing the pressure (decompression), the spectral positions and the shapes of all Raman bands return to the initial state (see Fig. 2b and Fig. S2, ESI†). The good convergence of the compression-decompression data indicates the reversibility of the high-pressure experiments. Such behavior is very important for optical pressure monitoring and implying the possibility of utilizing the synthesized SrGdAlO$_4$ material as an optical pressure gauge-manometer.

The luminescence properties of materials doped with Mn^{4+} ions are related to the electron transition from the excited ^{2}E state to the ground ^{4}A$_2$ state (Fig. 3a). The parabola of the ^{2}E level intersects with the ^{4}T$_2$ level at an energy called the activation energy (Δ*E*) and its value determines the thermal stability of the luminescence of Mn^{4+} ions, affecting the probability of non-radiative depopulation processes of the ^{2}E level. Since the energy of the ^{4}T$_2$ level strongly depends on the strength of the crystal field interacting with the Mn^{4+} ions,

the activation energy can be modified by appropriate selection of host material. To determine the strength of the crystal field for the SrGdAlO$_4$:Mn^{4+} structure, a well-known procedure based on the excitation band energies of Mn^{4+} ions is used (eqn S1–S4, ESI†).[28,38] As can be seen in Fig. 3b, the excitation spectra of the SrGdAlO$_4$:Mn^{4+} have three bands with maxima at around 300, 350, and 500 nm, corresponding to the Mn^{4+} → O^{2-}, ^{4}A$_2$ → ^{4}T$_1$, and ^{4}A$_2$ → ^{4}T$_2$ electronic transitions, respectively. It is clear that the spectral positions of the excitation bands do not significantly depend on the concentration of Mn^{4+} ions, and the determined strength of the crystal field is *Dq*/*B* = 2.36. However, with the increase in the dopant ion concentration, the intensity of the ^{4}A$_2$ → ^{4}T$_2$ band clearly increases compared to the other bands. The increase in the intensity of this band may explain the apparent change in the half-width of the ^{4}A$_2$ → ^{4}T$_1$ band, with increasing Mn^{4+} concentration. On the other hand, in the emission spectra, it can be seen that an increase in the concentration of Mn^{4+} ions causes a decrease in the intensity of the most intense component of the ^{2}E → ^{4}A$_2$ band, located at around 710 nm, in respect to the entire band, which is most likely related to the reabsorption process, the probability of which increases with a shortening of the average distance between adjacent Mn^{4+} ions (Fig. 3c). Since no significant changes in the spectroscopic properties of SrGdAlO$_4$:Mn^{4+} were found for different concentrations of Mn^{4+}, the SrGdAlO$_4$:0.2%Mn^{4+} sample was used as a representative material for further studies.

Investigating the effect of applied pressure on the luminescence properties of the SrGdAlO$_4$:0.2%Mn^{4+} material, the *in situ* luminescence spectra during the compression-decompression cycle were measured. An increase in pressure from ambient to ≈7.9 GPa leads to the spectral shift of the band maximum from 13976 cm^{-1} (715.66 nm) to 13861 cm^{-1} (721.44 nm) (Fig. 4a, see also Fig. S3, ESI†). The change in the position of this band can be discussed in terms of increasing covalency of the Mn^{4+}–O^{2-} bond, leading to a nephelauxetic red-shift,[39] which is an effect analogous to that used in the luminescence manometry of shifting the R$_1$ line of the ^{2}E → ^{4}A$_2$ band of Cr^{3+} ions in ruby.[11] The analysis of the excitation spectra of SrGdAlO$_4$:0.2%Mn^{4+} measured as a function of pressure indicates a blue shift of the Mn^{4+} absorption bands, which is associated with a change in the crystal field strength
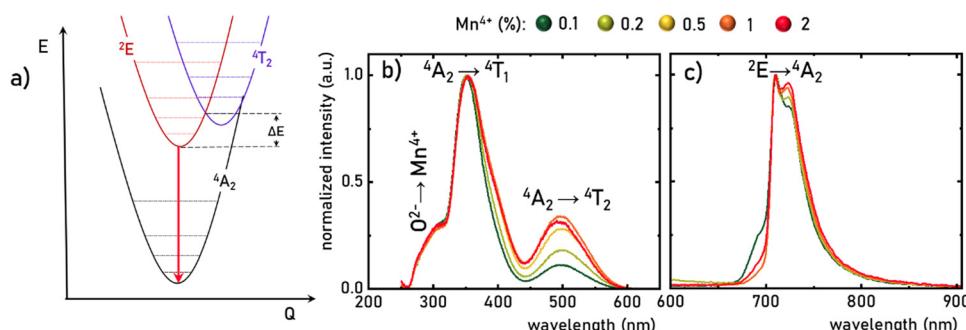
Fig. 3 Simplified configurational coordination diagram of Mn^{4+} ions (a), the comparison of the normalized room temperature excitation spectra (λ$_{em}$ = 710 nm) (b), and emission spectra (λ$_{exc}$ = 400 nm) (c) of SrGdAlO$_4$:Mn^{4+} with different concentration of Mn^{4+} ions.

11356 | *J. Mater. Chem. C*, 2023, **11**, 11353–11360

This journal is © The Royal Society of Chemistry 2023
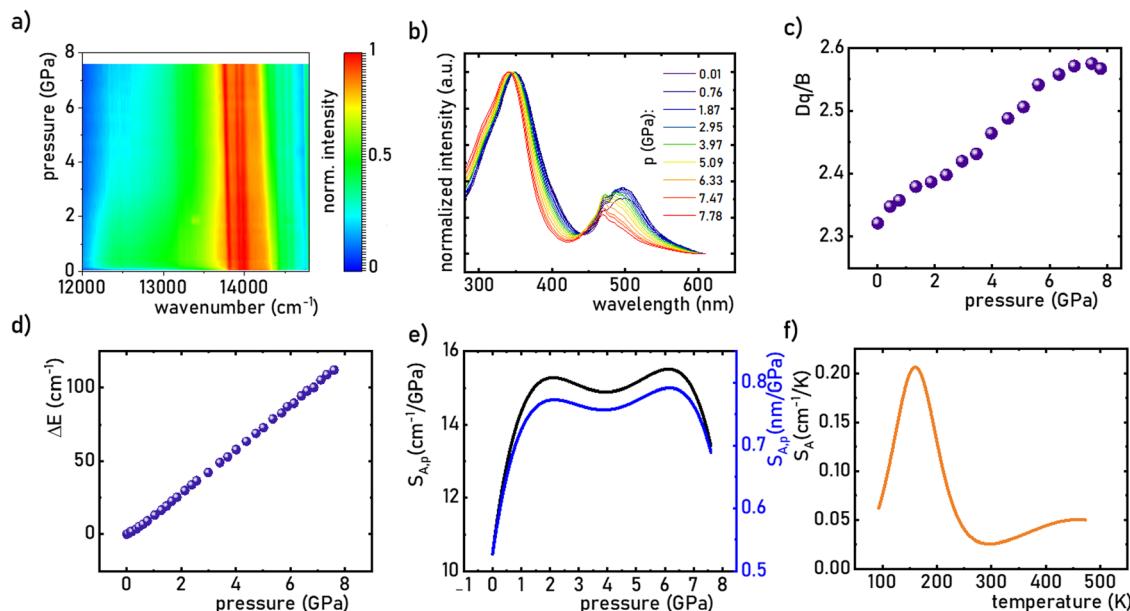
Fig. 4 The influence of the applied pressure on the normalized room temperature emission spectra of the $SrGdAlO_4 : 0.2\%Mn^{4+}$ (a); the excitation spectra of $SrGdAlO_4 : 0.2\%Mn^{4+}$ measured as a function of pressure (b); the change in the Dq/B as a function of applied pressure (c) determined change in the wavenumber of the emission band − ΔE (cm^{-1}) (d) and corresponding $S_{A,p}$ (e) as a function of pressure; $S_{A,T}$ as a function of temperature f).

(Fig. 4b and Fig. S4, ESI†). Calculation of the Dq/B parameter (where B is the Racah parameter) reveals the gradual increase of its value from 2.36 at ambient pressure up to 2.59 at 7.8 GPa (Fig. 4c). As can be seen, the band energy changes monotonically and varies by approx. 115 cm^{-1} (6.4 nm) in the analyzed pressure range (Fig. 4d), resulting in the absolute sensitivity determined as follows:

$$S_{A,p} = \frac{\Delta E}{\Delta p} \qquad (1)$$

$$S_{A,T} = \frac{\Delta E}{\Delta T} \qquad (2)$$

where ΔE is the change in the band energy corresponding to a change in pressure (temperature) by Δp (ΔT). The resulting $S_{A,p}$ value is ≈ 15.5 cm^{-1} GPa^{-1} at around 6 GPa that corresponds to $d\lambda/dp = 0.79$ nm GPa^{-1} and decreases with pressure (Fig. 4e). On the other hand, in the case of temperature measurements, the emission intensity decreases and the band position shifts slightly with temperature (Fig. S3a, ESI†). The maximum observed shift exceeds 25 cm^{-1} (Fig. S2b, ESI†). Making a pressure reading based on the spectral position of the $^2E \rightarrow ^4A_2$ band of Mn^{4+} ions is strongly affected by temperature change. Consequently, $SrGdAlO_4 : 0.2\%Mn^{4+}$ exhibits an absolute temperature sensitivity of about $S_{A,T} = 0.2$ cm^{-1} K^{-1} at 100 K, which decreases with increasing temperature (Fig. 4f). The corresponding $d\lambda/dT = 0.0097$ nm K^{-1} for $SrGdAlO_4 : 0.2\%$ Mn^{4+} is only slightly higher compared to 0.007 nm K^{-1} for ruby.

As already shown, the significant change in the $SrGdAlO_4 : 0.2\%Mn^{4+}$ luminescence intensity with temperature may suggest that the emission lifetime of the ^2E-excited level is strongly

thermally shortened. In order to experimentally verify this hypothesis, the luminescence decay profiles for the $SrGdAlO_4 : 0.2\%Mn^{4+}$ sample were measured in the range of 77–580 K (Fig. 5a and Fig. S5, ESI†). Due to the slight deviation of their shape from single-exponential profile, the average lifetimes (τ_{avr}) were determined according to the procedure described in ESI† (eqn S5 and S6, ESI†). At 77 K, the τ_{avr} equaled 2.1 ms and with increasing temperature it gradually shortened until 260 K, where it reached 1.61 ms. In the temperature range of 260–365 K, the τ_{avr} value remained almost constant (plateau), and above that threshold temperature a sharp reduction in the values was observed. A similar relationship for Mn^{4+} lifetimes was reported by Senden *et al*[40] for the $K_2TiF_6 : Mn^{4+}$ compound. According to the interpretation presented in the literature, this behavior can be explained in terms of a thermal change in the radiative lifetime of the ^2E state in the 77–365 K range, followed by the shortening associated with the nonradiative depopulation of the ^2E state at higher temperature values. The shortening of the radiative lifetime observed in the initial temperature range is due to the thermal population of odd-parity vibrational modes at elevated temperatures. The quantitative analysis of the obtained results was carried out by determining the relative sensitivity as follows:

$$S_{R,T} = \frac{1}{\tau_{avr}} \frac{\Delta \tau_{avr}}{\Delta T} \times 100\% \qquad (3)$$

$$S_{R,p} = \frac{1}{\tau_{avr}} \frac{\Delta \tau_{avr}}{\Delta p} \times 100\% \qquad (4)$$

where $\Delta\tau_{avr}$ represents the change in τ_{avr} corresponding to a change in temperature by ΔT (pressure by Δp). The obtained
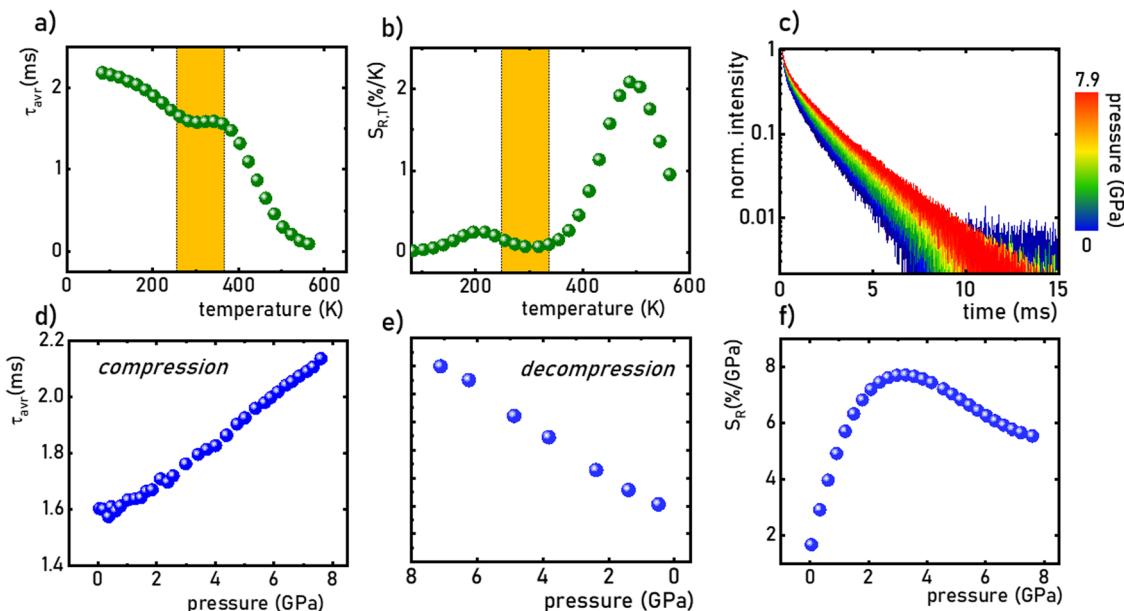
Fig. 5 The τ_{avr} of the SrGdAlO$_4$: 0.2%Mn^{4+} measured as a function of temperature (a) the corresponding $S_{R,T}$ (b); luminescence decay profile of SrGdAlO$_4$: 0.2%Mn^{4+} measured as a function of pressure (c); the τ_{avr} measured at room temperature as a function of pressure during compression (d) and decompression (e) and corresponding $S_{R,p}$ (f).

results indicate that the maximum sensitivity of $S_{R,T} = 2.1\%$ K^{-1} is observed at 490 K (Fig. 5b). However, in the 260–365 K T-range, $S_{R,T} < 0.09\%$ K^{-1}. This is direct evidence that the luminescence properties of the SrGdAlO$_4$: 0.2%Mn^{4+} compound in this T-range are temperature-independent. As the pressure increases, a significant elongation of the luminescence decay profiles was observed (Fig. 5c). In addition, it was noted that above 1.5 GPa the lifetime begins to approach a single-exponential profile with increasing pressure, and τ_{avr} monotonically increases with pressure from 1.44 ms up to 2.14 ms at 7.6 GPa (Fig. 5d and e). Importantly, its value shortens again during the decompression cycle, confirming that the observed changes are fully reversible, as shown previously in the Raman spectra. The observed effect can be explained by (i) a change in the probability of radiative processes resulting from a change in the covalency of the bond and depopulation of the odd-parity vibrational modes and (ii) a decrease in the probability of non-radiative processes through an increase in the activation energy resulting from an increase in the energy of the $^4T_2$ level. The analysis of the relative sensitivity of the lifetime-based manometer indicates that in the 1–7.6 GPa pressure range $S_{R,P} > 5\%$ GPa^{-1}, and the maximum value of $S_R = 7.85\%$ GPa^{-1} is reached at 3 GPa (Fig. 5f). This is a very high value comparable to the most sensitive luminescence manometers based on the spectral analysis of materials doped with Ln^{3+} ions.[41,42] However, it should be borne in mind that luminescence kinetics is hardly affected by the dispersive dependence of light absorption and scattering by the medium, and therefore allows for a more reliable measurement as proven for luminescence thermometry.[43] In the case of luminescence manometers, it is essential to provide a temperature-invariant pressure readout.

For this purpose, the temperature invariability manometric factor (TIMF) defined as follows was determined for the SrGdAlO$_4$: 0.2%Mn^{4+} sensor material:[44]

$$\text{TIMF} = \frac{S_{R,P}}{S_{R,T}} \qquad (5)$$

TIMF expresses the temperature change necessary to harness the change in spectroscopic properties corresponding to a 1 GPa change in pressure. The larger the TIMF value, the more temperature-independent the pressure reading. In the case of the SrGdAlO$_4$: 0.2%Mn^{4+} compound compressed to 2.1 GPa at room temperature, the TIMF is 134, which is the final confirmation of the high application potential of this material. Additional advantage of this manometer is the fact that τ_{avr} shows very high repeatability within the compression and decompression cycles (Fig. S6, ESI†). The calculation of the pressure determination uncertainty (eqn S7, ESI†) for lifetime-based luminescence manometry on SrGdAlO$_4$: 0.2%Mn^{4+} was as low as 0.07 GPa at 3 GPa, which confirms a high manometric performance of this luminescence manometer.

Conclusions

In this study, the spectroscopic properties of the SrGdAlO$_4$: 0.2%Mn^{4+} material were studied as a function of pressure and temperature to develop a lifetime-based luminescent manometer. It was shown that the $^2E \rightarrow {}^4A_2$ emission spectral band shifts with applied pressure, with the maximum absolute sensitivity $S_{A,p} \approx 15.5$ cm^{-1} GPa^{-1} at around 6 GPa (dλ/dp = 0.79 nm GPa^{-1}) and temperature with $S_{A,T} = 0.2$ cm^{-1} K^{-1} at 200 K. The luminescence intensity of the Mn^{4+} emission is

11358 | *J. Mater. Chem. C*, 2023, **11**, 11353–11360

This journal is © The Royal Society of Chemistry 2023

rapidly quenched with temperature, indicating that the activation energy, and thus the energy of the $^4T_2$ band is probably relatively low. Measurements of lifetimes as a function of temperature reveal that in the range of 77–360 K the change in lifetime values result from a change in the probability of radiative processes. Whereas, the rapid shortening of the τ_{avr} values observed above 360 K originates from an increase in the probability of non-radiative processes. Importantly, in the range of 260–360 K the τ_{avr} remains insensitive to temperature changes. The pressure-dependence analysis indicates that the τ_{avr} values significantly and monotonically prolong with pressure, at least up to ≈ 7.9 GPa, and the maximum sensitivity reaches $S_{R,p} = 7.85\%$ GPa^{-1} at 3 GPa with the pressure determination uncertainty as low as 0.07 GPa at 3 GPa. Importantly, the observed changes in lifetime values are fully reversible. The high value of the TIMF parameter (≈ 134) confirms the high application potential of the SrGdAlO$_4$:0.2%Mn^{4+} material for remote pressure readings based on the lifetime of the ^2E excited state. We believe this study can trigger research interest in the use of Mn^{4+} doped phosphors to develop a new class of highly reliable luminescent manometers.

Conflicts of interest

There are no conflicts to declare.

Acknowledgements

References

1 Z. Hu, B. J. Deibert and J. Li, *Chem. Soc. Rev.*, 2014, **43**, 5815–5840.

2 S. V. Eliseeva and J.-C. G. Bünzli, *Chem. Soc. Rev.*, 2010, **39**, 189–227.

3 O. S. Wolfbeis, *Anal. Chem.*, 2006, **78**, 3859–3874.

4 M. D. Dramićanin, *J. Appl. Phys.*, 2020, **128**, 40902.

5 L. Marciniak, K. Kniec, K. Elżbieciak-Piecka, K. Trejgis, J. Stefanska and M. Dramićanin, *Coord. Chem. Rev.*, 2022, **469**, 214671.

6 X. D. Wang, O. S. Wolfbeis and R. J. Meier, *Chem. Soc. Rev.*, 2013, **42**, 7834–7869.

7 B. R. Jovanić and J. P. Andreeta, *Phys. Scr.*, 1999, **59**, 274–276.

8 T. Zheng, L. Luo, P. Du, S. Lis, U. R. Rodríguez-Mendoza, V. Lavín, I. R. Martín and M. Runowski, *Chem. Eng. J.*, 2022, **443**, 136414.

9 M. Szymczak, P. Woźny, M. Runowski, M. Pieprz, V. Lavín and L. Marciniak, *Chem. Eng. J.*, 2023, **453**, 139632.

10 R. R. Petit, S. E. Michels, A. Feng and P. F. Smet, *Light: Sci. Appl.*, 2019, **8**, 124.

11 H. K. Mao, J. Xu and P. M. Bell, *J. Geophys. Res.*, 1986, **91**, 4673.

12 M. Tian, Y. Gao, P. Zhou, K. Chi, Y. Zhang and B. Liu, *Phys. Chem. Chem. Phys.*, 2021, **23**, 20567–20573.

13 Y. Masubuchi, S. Nishitani, S. Miyazaki, H. Hua, J. Ueda, M. Higuchi and S. Tanabe, *Appl. Phys. Express*, 2020, **13**, 42009.

14 J. Liu and Y. K. Vohra, *Appl. Phys. Lett.*, 1994, **64**, 3386–3388.

15 Y. R. Shen, T. Gregorian and W. B. Holzapfel, *High Pressure Res.*, 1991, **7**, 73–75.

16 B. Lorenz, Y. R. Shen and W. B. Holzapfel, *High Pressure Res.*, 1994, **12**, 91–99.

17 F. H. Su, Z. L. Fang, B. S. Ma, K. Ding, G. H. Li and W. Chen, *J. Phys. Chem. B*, 2003, **107**, 6991–6996.

18 N. J. Hess and G. J. Exarhos, *High Pressure Res.*, 1989, **2**, 57–64.

19 J. Barzowska, T. Lesniewski, S. Mahlik, H. J. Seo and M. Grinberg, *Opt. Mater.*, 2018, **84**, 99–102.

20 U. R. Rodríguez-Mendoza, S. F. León-Luis, J. E. Muñoz-Santiuste, D. Jaque and V. Lavín, *J. Appl. Phys.*, 2013, **113**, 213517.

21 L. M. M. Szymczak, M. Runowski and V. Lavín, *Laser Photonics Rev.*, 2023, **17**, 2200801.

22 M. Pieprz, M. Runowski, K. Ledwa, J. J. Carvajal, A. Bednarkiewicz and L. Marciniak, *ACS Appl. Opt. Mater.*, 2023, **1**, 1080–1087.

23 L. Labrador-Páez, M. Pedroni, A. Speghini, J. García-Solé, P. Haro-González and D. Jaque, *Nanoscale*, 2018, **10**, 22319–22328.

24 A. Bednarkiewicz, L. Marciniak, L. D. Carlos and D. Jaque, *Nanoscale*, 2020, **12**, 14405–14421.

25 M. Runowski, J. Marciniak, T. Grzyb, D. Przybylska, A. Shyichuk, B. Barszcz, A. Katrusiak and S. Lis, *Nanoscale*, 2017, **9**, 16030–16037.

26 Q. Zhou, L. Dolgov, A. M. Srivastava, L. Zhou, Z. Wang, J. Shi, M. D. Dramićanin, M. G. Brik and M. Wu, *J. Mater. Chem. C*, 2018, **6**, 2652–2671.

27 M. G. Brik and A. M. Srivastava, *J. Lumin.*, 2013, **133**, 69–72.

28 M. G. Brik, S. J. Camardello and A. M. Srivastava, *ECS J. Solid State Sci. Technol.*, 2015, **4**, R39.

29 M. Pechini, US Pat., US3330697A, 1967.

30 T. Zheng, M. Sójka, P. Woźny, I. R. Martín, V. Lavín, E. Zych, S. Lis, P. Du, L. Luo and M. Runowski, *Adv. Opt. Mater.*, 2022, **10**, 2201055.

31 W. Xie, J. Feng, X. Liu, L. Yan, H. Guo, Y. Dai, Y. Xie, H. S. Jang and J. Lin, *J. Alloys Compd.*, 2018, **753**, 781–790.

32 A. Hooda, S. P. Khatkar, A. Khatkar, S. Chahar, S. Devi, J. Dalal and V. B. Taxak, *Curr. Appl. Phys.*, 2019, **19**, 621–628.

33 P. Sehrawat, A. Khatkar, A. Hooda, M. Kumar, R. Kumar, R. K. Malik, S. P. Khatkar and V. B. Taxak, *Ceram. Int.*, 2019, **45**, 24104–24114.

34 A. Hooda, S. P. Khatkar, A. Khatkar, R. K. Malik, J. Dalal, S. Devi and V. B. Taxak, *Mater. Chem. Phys.*, 2019, **232**, 39–48.

This journal is © The Royal Society of Chemistry 2023

J. Mater. Chem. C, 2023, **11**, 11353–11360 | **11359**

35 F. Zou, M. Li, Z. Du, Y. Song, L. Li and G. Li, *Opt. Mater.*, 2022, **133**, 112904.

36 A. Hooda, S. P. Khatkar, A. Khatkar, M. Kumar, M. Dalal and V. B. Taxak, *J. Mater. Sci.: Mater. Electron.*, 2019, **30**, 1297–1309.

37 Q. Sun, S. Wang, B. Devakumar, B. Li, L. Sun, J. Liang, D. Chen and X. Huang, *RSC Adv.*, 2018, **8**, 39307–39313.

38 M. G. Brik, S. J. Camardello, A. M. Srivastava, N. M. Avram and A. Suchocki, *ECS J. Solid State Sci. Technol.*, 2016, **5**, R3067.

39 T. Zheng, L. Luo, P. Du, S. Lis, U. R. Rodríguez-Mendoza, V. Lavín and M. Runowski, *Chem. Eng. J.*, 2022, **446**, 136839.

40 T. Senden, R. J. A. Van DIjk-Moes and A. Meijerink, *Light: Sci. Appl.*, 2018, **7**, 8.

41 M. Sójka, M. Runowski, P. Woźny, L. D. Carlos, E. Zych and S. Lis, *J. Mater. Chem. C*, 2021, **9**, 13818–13831.

42 M. A. Antoniak, S. J. Zelewski, R. Oliva, A. Żak, R. Kudrawiec and M. Nyk, *ACS Appl. Nano Mater.*, 2020, **3**, 4209–4217.

43 M. Runowski, S. Goderski, D. Przybylska, T. Grzyb, S. Lis and I. R. Martín, *ACS Appl. Nano Mater.*, 2020, **3**, 6406–6415.

44 M. Szymczak, M. Runowski, M. G. Brik and L. Marciniak, *Chem. Eng. J.*, 2023, 143130.

11360 | *J. Mater. Chem. C,* 2023, **11**, 11353–11360

This journal is © The Royal Society of Chemistry 2023